Phase Diagram for a Diblock Copolymer Melt under Cylindrical Confinement

Weihua Li, Robert A. Wickham,* and Robert A. Garbary

Department of Physics, St. Francis Xavier University, Antigonish, Nova Scotia, Canada B2G 2W5

ABSTRACT: We extensively study the phase diagram of a diblock copolymer melt confined in a cylindrical nanopore using real-space self-consistent mean-field theory. We discover a rich variety of new two-dimensional structures that have no analogue in the unconfined system. These include nonhexagonally coordinated cylinder phases and structures intermediate between lamellae and cylinders. We map the stability regions and phase boundaries for all the structures we find. As the pore diameter is decreased, the pore accommodates fewer cylindrical domains and structural transitions occur as cylinders are eliminated. Our results are consistent with experiments, but we also predict phases yet to be observed.

I. Introduction

Self-assembly in macromolecular systems provides a convenient route to create structure at the nanoscale. These structures have potential applications as, for example, lithographic templates for nanowires, photonic crystals, and high-density magnetic storage media.[1] Confinement effects, produced by boundaries, influence the self-assembly process and can generate novel nanostructures. In a rational search for new morphologies to fit a particular application, it is crucial to know which structures are possible in a confined system and under what conditions; i.e., one needs to know the phase diagram.

Confined diblock copolymer melts have become the focus of increasing attention. In the bulk, these materials self-assemble into a variety of periodic nanostructures—lamellae, hexagonally coordinated cylinders, body-centered cubic lattices of spheres, and the gyroid morphology. The ability to tune the period and to control self-assembly using temperature, chemical composition, and molecular architecture lend a rich physics to these materials and make them attractive for industrial applications.[1–4] Competition between the chain stretching energy and the interfacial energy between block domains determines which structures form in the bulk. Introducing confinement modifies this competition. Confinement of diblock copolymers between parallel solid walls, or in a thin film, has been extensively studied.[5–9] However, the effect of confinement in a cylindrical pore is relatively unexplored.

Recently, Xiang et al. examined asymmetric and symmetric polystyrene-*b*-polybutadiene (PS-*b*-PBD) diblock copolymers confined to cylindrical alumina nanopores and observed cylindrical and concentric lamellar structures in the pores.[10] Concentric lamellar structures were also seen in the experiments of Sun et al. involving symmetric polystyrene-*b*-poly(methyl methacrylate) (PS-*b*-PMMA) diblock copolymers confined in alumina nanopores.[11] Concentric lamellar structures have been seen in the Monte Carlo simulations of He et al.[12] and in the dynamical density functional simulations of Sevink et al.[13] Experiments using narrower pores find that stacked-disk or toroidal-type structures, and also helical cylinders, are possible.[14,15] Such three-dimensional structures have been seen in the simulations of ref 13 and in a self-consistent mean-field

theory (SCMFT) study of self-assembled silica–surfactant mesostructures in cylindrical nanopores.[16] However, in all the simulation and theoretical work to date, only a few phases, in a very limited region of parameter space, have been studied due to the time and computational requirements. Knowledge of the phase behavior of cylindrically confined block copolymers is thus currently fragmentary.

To fill this knowledge gap, we systematically evaluate the phase diagram for a diblock copolymer melt confined in a cylindrical nanopore using SCMFT. SCMFT has proved to be one of the most successful theoretical methods for investigating equilibrium phases in block copolymers and has played a major role in establishing the phase diagram of the bulk diblock copolymer melt.[17,18] We explore the phase diagram for the cylindrically confined melt and identify the equilibrium phase boundaries and stability regions for various phases that exist in this system. We consider structures that are translationally invariant along the pore axis and are thus two-dimensional. Previous works have examined on the order of 10 points in the phase diagram. Our study examines ~3000 points in the phase diagram and consumes ~15 000 CPU hours on a 3 GHz Intel Xeon processor. The resolution of our study enables us to observe the intricate nature of the phase diagram, which is more complex than that for the bulk system.

II. Theory

We consider an incompressible melt of AB diblock copolymers, confined to a cylindrical pore of radius R. Each copolymer has a degree of polymerization N while the A-block on each has a degree of polymerization fN with $0 \leq f \leq 1$. Lengths in our theory are expressed in units of the radius of gyration, R_g, of the polymer. Within the mean-field approximation to the many-chain Edwards theory,[19,20] at a temperature T the free energy F for n Gaussian diblock copolymer chains confined in a cylindrical pore has the form

$$\frac{F}{nk_BT} = -\ln Q + \frac{1}{V}\int_{|\mathbf{r}|\leq R}d\mathbf{r}\,\{\chi N\phi_A(\mathbf{r})\,\phi_B(\mathbf{r}) - \omega_A(\mathbf{r})\,\phi_A(\mathbf{r}) - \omega_B(\mathbf{r})\,\phi_B(\mathbf{r}) + H(\mathbf{r})[\phi_A(\mathbf{r}) - \phi_B(\mathbf{r})]\} \quad (1)$$

The monomer densities are ϕ_A and ϕ_B; the partition function Q is for a single polymer interacting with the mean fields ω_A and ω_B produced by the surrounding chains. These quantities have

* Corresponding author. E-mail: rwickham@stfx.ca.

CDV

the standard definitions and meanings.[17,18] The Flory–Huggins interaction parameter, χ, characterizes the repulsion between dissimilar monomers. In the confined melt, the spatial integration is restricted to the pore volume, taken to be V.

We assume the pore wall has a preference for B monomers and include a surface field $H(\mathbf{r})$ in eq 1 that attracts species B. For convenience, this surface field is chosen to have the form

$$\frac{H(\mathbf{r})}{\chi N} = V_0\{\exp[(\sigma + |\mathbf{r}| - R)/\lambda] - 1\} \quad (2)$$

for $R - \sigma \leq |\mathbf{r}| \leq R$, while $H(\mathbf{r}) = 0$ for $|\mathbf{r}| < R - \sigma$. We choose the cutoff distance for the surface interaction to be $\sigma = 0.4R_g$ and the decay length to be $\lambda = 0.2R_g$. We fix the strength of the surface field to be $V_0 = 0.4$. In this study, we choose to focus on the influence of temperature (through χN) and f on the morphology, rather than the influence of the surface field. In experiments, a preferential interaction between the pore wall and the B monomers is known to exist but has not been characterized.[10] We have studied the effect of modest variations in V_0 ($0.1 \leq V_0 \leq 0.4$) on a few phase transition curves in our system and found that such variations did not significantly influence the morphologies and transition curves.

Minimization of the free energy with respect to the monomer densities and mean-fields leads to the set of mean-field equations

$$\omega_A(\mathbf{r}) = \chi N \phi_B(\mathbf{r}) + H(\mathbf{r}) + \eta(\mathbf{r}) \quad (3)$$

$$\omega_B(\mathbf{r}) = \chi N \phi_A(\mathbf{r}) - H(\mathbf{r}) + \eta(\mathbf{r}) \quad (4)$$

$$\phi_A(\mathbf{r}) = \frac{1}{Q}\int_0^f ds\, q(\mathbf{r},s)\, q^\dagger(\mathbf{r},s) \quad (5)$$

$$\phi_B(\mathbf{r}) = \frac{1}{Q}\int_f^1 ds\, q(\mathbf{r},s)\, q^\dagger(\mathbf{r},s) \quad (6)$$

with

$$Q = \frac{1}{V}\int_{|\mathbf{r}| \leq R} d\mathbf{r}\, q(\mathbf{r},s)\, q^\dagger(\mathbf{r},s) \quad (7)$$

Incompressibility

$$\phi_A(\mathbf{r}) + \phi_B(\mathbf{r}) = 1 \quad (8)$$

is enforced via the Lagrange multiplier $\eta(\mathbf{r})$, for $|\mathbf{r}| < R$. A key quantity appearing in these equations is the end-segment distribution function $q(\mathbf{r},s)$, which is proportional to the probability that a polymer chain segment, of contour length s and with one free end, has its other end located at $\mathbf{r}$. Both this distribution function and its conjugate, $q^\dagger(\mathbf{r},s)$, satisfy the modified diffusion equations

$$\frac{\partial q(\mathbf{r},s)}{\partial s} = \nabla^2 q(\mathbf{r},s) - \omega(\mathbf{r},s)\, q(\mathbf{r},s) \quad (9)$$

$$-\frac{\partial q^\dagger(\mathbf{r},s)}{\partial s} = \nabla^2 q^\dagger(\mathbf{r},s) - \omega(\mathbf{r},s)\, q^\dagger(\mathbf{r},s) \quad (10)$$

with $\omega(\mathbf{r},s) = \omega_A(\mathbf{r})$ for $0 \leq s \leq f$ and $\omega(\mathbf{r},s) = \omega_B(\mathbf{r})$ for $f < s \leq 1$. The initial conditions are $q(\mathbf{r},0) = 1$ and $q^\dagger(\mathbf{r},1) = 1$. Equations 3–10 can be solved self-consistently in real space to find the equilibrium densities.[17,18,21] We employ the split-step Fourier method of Tzeremes et al.[22] to solve the modified diffusion equations for the end-segment distribution functions on a 128×128 square lattice, with a lattice constant of $0.136R_g$.

The chain contour length for each block is discretized into 128 segments. We find that the stability regions and phase boundaries are not significantly altered if we use a finer mesh, indicating that a 128×128 lattice provides sufficient accuracy.[23] Outside the pore, $|\mathbf{r}| \geq R$, there is no polymer, so we set the end-segment distribution functions to zero outside the pore, which implies that $\phi_A = \phi_B = 0$ in this region.[24] The sides of the square lattice are slightly larger than the diameter of the cylindrical pore. We impose periodic boundary conditions on all edges of the square and employ the standard fast Fourier transform algorithm over the square lattice.[25] Since the monomer densities and end-segment distributions are zero outside the cylinder, we expect the periodic images of the pore will not influence behavior in the pore. When we increase the physical box size, keeping the pore size fixed, our results are unchanged, suggesting this is the case.

Other than assuming that the structures are translation-invariant along the axis of the pore, we do not make any a priori assumptions about the symmetry of potential equilibrium structures. This is a major advantage of the real-space approach.[21] We first use random initial conditions in our iterative algorithm to generate a large set of solutions to the mean-field equations over a wide region of phase space. Once we determine this set, we then use these solutions as initial conditions in our algorithm to explore the extent (if any) of their stability regions. We take the equilibrium phase to be the structure which has the lowest free energy, for a given f and χN, of all the observed structures.

III. Results and Discussion

We first examine the phases that form in a fixed pore radius, $R = 8.5R_g$, and later discuss results for different radii (diameters). The 21 equilibrium nanostructured phases found at this pore radius are shown in Figure 1. The notation we use for the structures is explained in the caption of Figure 1. The phase diagram is presented in Figure 2 and has some features in common with the phase diagram for the unconfined diblock copolymer melt.[17] The disordered (D) phase is stable when χN is low or when the copolymer is close to being a homopolymer ($f \to 0$ or 1). Above the order–disorder transition, for $f \lesssim 0.3$, the asymmetry in the block composition favors curved interfaces and the formation of cylindrical[26] domains of the minority A species. Inverted cylindrical domains, composed of the minority B species, form when $f \gtrsim 0.65$. Symmetric copolymers favor AB interfaces with low curvature and thus concentric lamellar rings form in the center of the phase diagram. There are, however, significant differences between our phase diagram and the phase diagram for the bulk system, which we now discuss.

Our phase diagram is much more intricate than the phase diagram for the unconfined melt. Many of the trends in the phase diagram can be understood in terms of packing a finite number of domains into the pore, which has a finite cross-sectional area. For a given R, f, and χN, there is an optimum number of domains that can be accommodated—this number minimizes the free energy penalties associated with AB interfaces and chain stretching (or compression). At fixed R, as χN increases, we see from Figures 1 and 2 that the domain size increases, and the number of domains in the pore decreases. For example, as χN increases at fixed $f = 0.22$ the structure changes from C_{1-6-13} to C_{1-6-11} to C_{1-5-11} to C_{4-10}. A similar trend is seen for the inverted cylinder phases and for the concentric lamellae. For the cylinder phases of minority A (B) species, a similar argument explains the trends with increasing (decreasing) f. These packing considerations are purely the result of confinement and do not arise in the bulk.

CDV

C_{4-10} C_{1-5-11} C_{1-6-11} C_{1-6-12} C_{1-6-13} C_{0-0-13}

$a: LC_3$ $b: LC_{L,1}$ $c: LC_{LL}$ $d: LC_{L,2}$ $e: LC_4$ LC_{1-5}

LC_{1-6} L_2 L_3 $L\bar{C}_2$ $\bar{C}_{1-6}$ $\bar{C}_{1-7}$

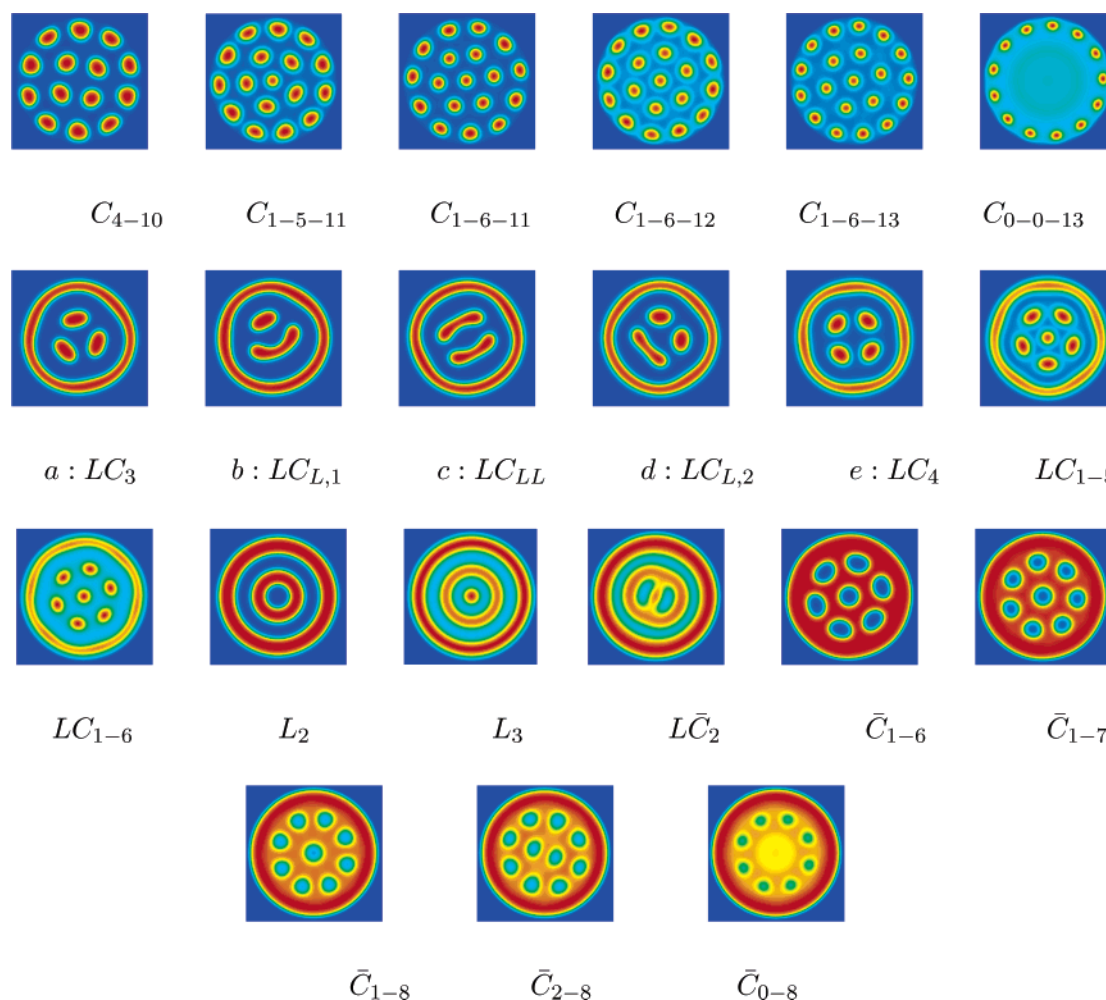$\bar{C}_{1-8}$ $\bar{C}_{2-8}$ $\bar{C}_{0-8}$

Figure 1. Monomer density plots of the 21 nanostructured phases formed in the $8.5R_g$ radius pore. The color ranges from deep red (A-rich regions) to deep blue (B-rich regions). The region outside the cylindrical pore is also colored deep blue. We use the notation C for cylindrical phases, L for lamellar phases, and LC for structures containing both lamellae and cylinders, which we call "intermediate phases". When the cylinders are composed of minority B component, an overbar ($\bar{C}$ or $L\bar{C}$) is used. The number of cylinders in each ring, out from the center of the pore, is indicated by subscripts C_{i-j-k}. The number of L subscripts in the notation $LC_{L\cdots L, i-j}$ indicates the number of lamellar segments in the inner region of a given intermediate structure. The second subscript indicates the number of cylinders of the minority species in the pore and whether these cylinders are arranged in rings. The stability regions for these structures are labeled on the phase diagram in Figure 2. The notation (a, b, c, d, e) is used to label some of the intermediate phases in Figure 2.

We observe arrangements of cylinders in the inner region of the pore with nonhexagonal coordination, such as the C_{4-10}, C_{1-5-11}, and $\bar{C}_{1-7}$ phases. Cylindrical structures with nonhexagonal coordination are not seen as equilibrium phases in the bulk, since such structures produce a highly nonuniform majority domain thickness, with an associated free energy penalty.[18] Our observation of nonhexagonally coordinated cylinders suggests that, when confined, the system will tolerate a nonuniform majority domain thickness if it can avoid the compression (or stretching) penalty of packing a nonoptimum number of cylinders into the pore.

For a narrow region $0.3 \lesssim f \lesssim 0.4$ in Figure 2 we see structures that are intermediate between cylinders and lamellae (this region is enlarged in Figure 3). As in the unconfined melt, a value of f closer to 0.5 favors AB interfaces of lower curvature. For example, for $\chi N = 23$, as f increases above $f \approx 0.3$, the C_{4-10} structure will transform into LC_4 as the presence of the pore wall first leads the outer ring of cylinders to coalesce into a single narrow domain of the A phase. With increasing f, the AB interfacial curvature is lowered further as cylinders coalesce into lamellar segments in the inner region, and the system transforms to the $LC_{L,2}$ and then LC_{LL} phases. When f increases above $f \approx 0.4$, the high curvature of the semicircular end-caps

on the lamellar segments becomes unfavorable, leading to the formation of concentric lamellar rings. Like the gyroid phase in the unconfined diblock copolymer melt, these intermediate phases represent a compromise between pure cylindrical and pure lamellar order.

We check that these intermediate phases are not artifacts of the discretization scheme by examining these phases with larger lattices (256×256 and 512×512). The physical pore radius, $R = 8.5R_g$, is held fixed. As Figure 3 shows, the phase boundaries between the intermediate structures in this region are not altered significantly when a finer mesh is used.[23] When the lattice size is changed, we do observe small differences in the density profile in AB interfacial regions. The finer mesh more accurately represents the rapid spatial variations of the density in these regions. These results increase our confidence that these intermediate structures are equilibrium structures, within the set of two-dimensional structures. We discuss the important question of the existence three-dimensional structures at the end of this section.

There is an asymmetry in the phase diagram, arising from the preference of the pore wall for the B block. In Figures 1 and 2 the arrangements of the inverted cylinders and the stability regions for these structures are less complicated than the
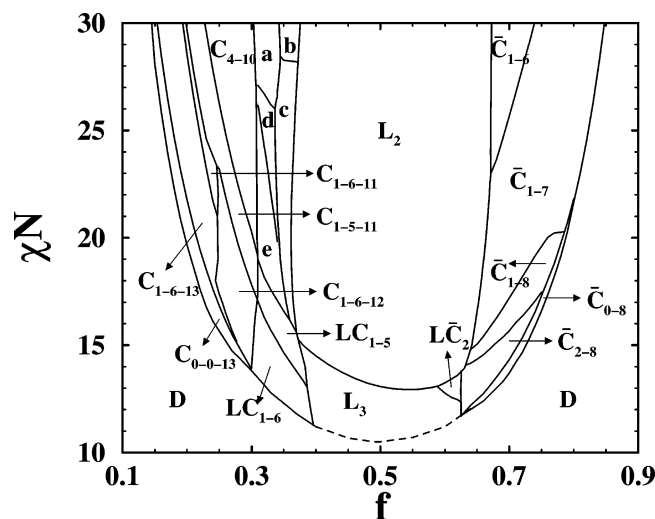
CDV

Figure 2. Phase diagram for a diblock copolymer melt confined in a cylindrical nanopore of radius $R = 8.5R_g$. The degree of polymerization of the copolymer is N, the Flory−Huggins parameter is χ, and f is the A monomer fraction. The disordered phase is labeled D; the other labels are as in Figure 1. The dashed curve is an interpolation of the order−disorder transition curve, as explained in the text.
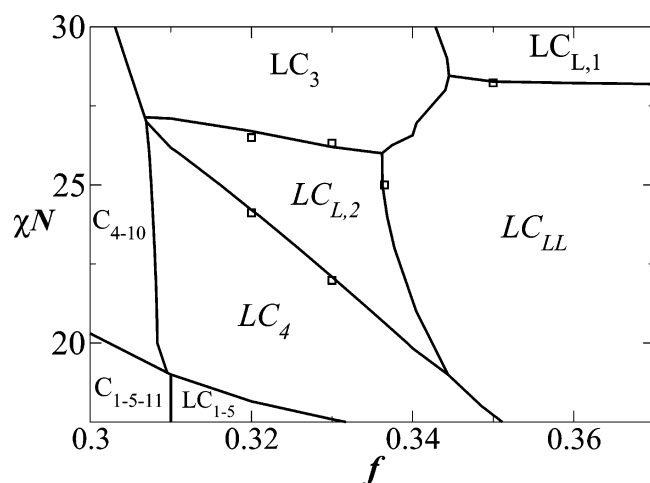

Figure 3. Focus on the region of Figure 2 where intermediate phases exist in the $R = 8.5R_g$ pore. The structures are labeled as in Figure 1. Solid curves represent structural phase transitions determined using a 128×128 lattice, as in Figure 2. Squares represent phase transition points determined using a 256×256 lattice.

cylindrical structures seen for $f \lesssim 0.3$. One can think about the behavior in this region in terms of the behavior for $f \lesssim 0.3$ by exchanging the A and B monomers and recognizing that the inverted cylinders exist in a pore with a smaller effective radius. In the inverted cylinder phases, a thick double layer of A monomers exists between the thin layer of minority B block along the pore wall and the cylinders in the inner region. We suggest that the outer A block, attached to the B block along the actual pore wall, acts as filler, creating an effective pore wall (of smaller radius) with a preference for A. As we see below, when the diameter of the pore decreases, fewer cylinders form in the pore.

All the order−order transitions we observe are first-order phase transitions. An example of a typical free energy curve near an order−order transition is shown in Figure 4a. As the order−disorder transition (ODT) is approached, the inner region can disorder first (the C_{1-6-13} to C_{0-0-13} transition, for example) before the final transition to disorder. The free energy curve for the transition from C_{0-0-13} to D at $f = 0.16$ is shown in
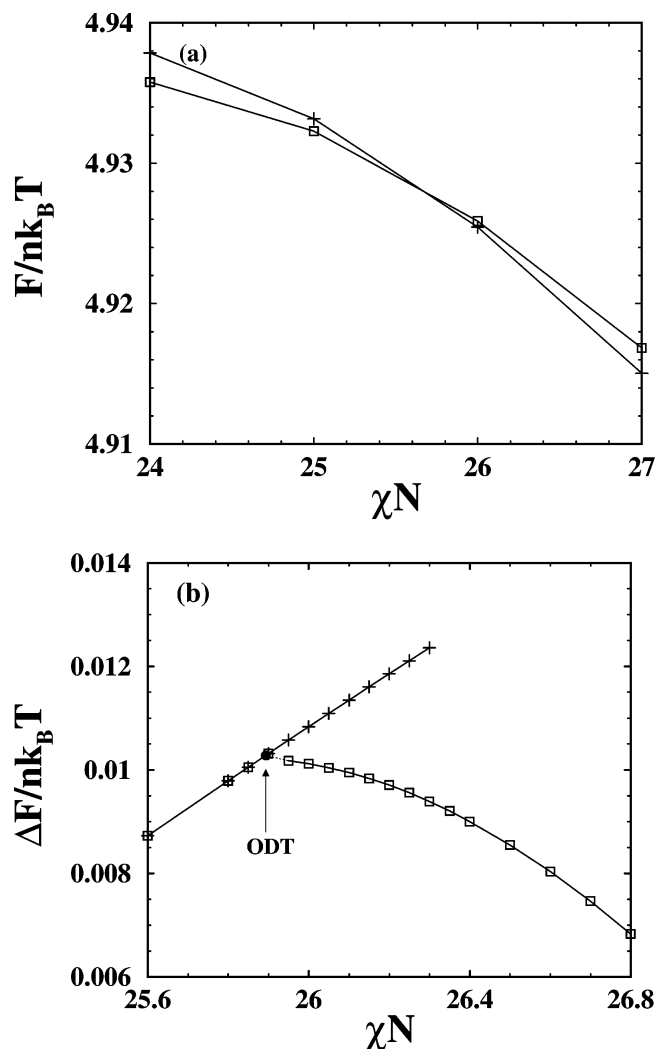

Figure 4. Typical free energy curves as a function of χN near phase transitions occurring in Figure 2. (a) Free energies of the $\bar{C}_{1-6}$ (cross) and $\bar{C}_{1-7}$ (square) phases at $f = 0.7$. (b) Free energies for the C_{0-0-13} phase (squares) and disordered phase (crosses) for $f = 0.16$. In (b) we shift the free-energies, F, for clarity and display the quantity $\Delta F/nk_BT = F/nk_BT - [3(\chi N - 25.6)/70 + 3.32]$. The order−disorder transition point is denoted ODT. On increasing χN, the disordered phase remains metastable beyond the ODT but eventually transforms into the C_{0-0-13} phase.

Figure 4b. The ODT is first order, except perhaps for the ODT from L_3 to D. We are unable to determine the location of the ODT from L_3 to D, as there appears, in this case, to be no feature in the free energy at the ODT. The dashed curve shown in Figure 2 is an interpolation of the full ODT curve. As the L_3 to D transition is approached along the ODT, from high or low f, the first-order ODT becomes weaker. We recently began a study of the ODT near $f = 0.5$ using reciprocal-space SCMFT.[27] Our preliminary results suggest that in the absence of a surface field the ODT from L_3 to D is second order and occurs at a well-defined value of χN, which depends on f. However, when there is a surface field, the transition from L_3 to D appears as a crossover due to the influence of the surface field on the monomer densities. Presumably this crossover behavior will disappear, and a well-defined ODT point will emerge as the pore size is increased.

We explore the effect of changing the pore diameter $D = 2R$ for the phase-space point $f = 0.26$ and $\chi N = 20$. Our results are shown in Figure 5. With increasing pore diameter, the complexity of the structures, in terms of both number of
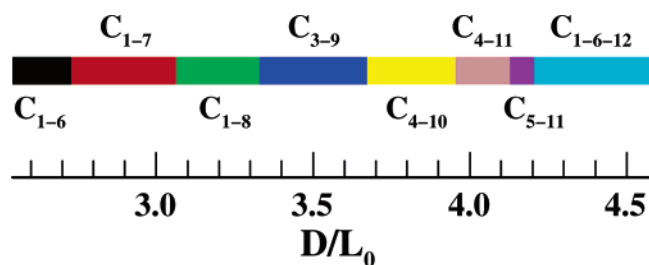
CDV

Figure 5. Phase stability regions for cylindrical structures at $f = 0.26$ and $\chi N = 20$ as a function of pore diameter D. The diameter is scaled in units of the equilibrium distance between hexagonally coordinated cylinders in the bulk, $L_0 = 3.934R_g$, determined from reciprocal-space SCMFT at this χN and f. Colors indicate the stability range for each of the structures indicated, as the diameter of the cylindrical pore is varied.
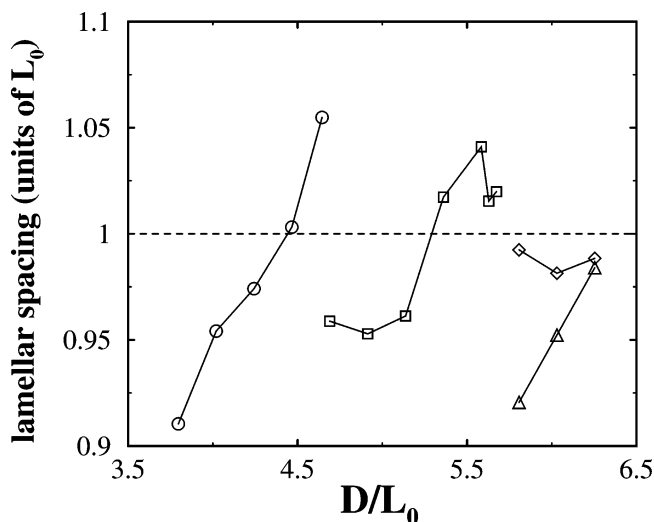

Figure 6. Spacing between concentric lamellae of species A, at $f = 0.5$ and $\chi N = 30$, as a function of the pore diameter D. Both the pore diameter and the lamellar spacing are scaled in units of the equilibrium, bulk lamellar period, $L_0 = 4.477R_g$, determined from reciprocal-space SCMFT at this χN and f. Circles correspond to the L_2 structure in Figure 1. Squares correspond to to L_2 structure, with the central domain of B transformed into a central domain of A, surrounded by a ring of B. Diamonds and triangles correspond to structures with three lamellae of species A, with a central circular region of B. Diamonds represent the difference between the radii of the middle and inner A layer, and triangles represent the difference between the radii of the outer and middle A layer.

cylinders and the number of rings, increases. We observe the effect of commensurability of the pore diameter with the hexagonal arrangement of cylinders expected in the bulk—the C_{1-6} phase appears in smaller pores and then, following intervening, nonhexagonal phases reappears as the C_{1-6-12} phase in larger pores. Our expectation is that, for larger pore sizes, a hexagonal array of cylinders will preferentially form in the inner region of the pore in order to minimize unfavorable nonuniformities in the majority domain thickness. The C_{1-6}, C_{1-7}, and C_{1-8} phases we observe here correspond, when A is exchanged with B, to structures seen in Figure 2 for $f \gtrsim 0.65$, supporting the idea that these latter structures form due to confinement in a pore with a smaller effective size.

In Figure 6, we show the difference between the radii of concentric lamellae of species A as a function of the pore diameter D for $f = 0.5$ and $\chi N = 30$. When there are three lamellae of species A in the pore, we show both the difference between the radii of the middle and inner layer and the difference between the radii of the outer and middle layer. We determine the lamellar period, $L_0 = 4.477R_g$, for the unconfined melt using reciprocal-space SCMFT and display it as the dashed

line in Figure 6. As the pore diameter increases, we observe regions of compression or expansion of the lamellae about the unconfined period, as the lamellar spacing adjusts to fit a fixed number of lamellae into to the pore. At $D \approx 4.6L_0$ there is a jump in the lamellar spacing as the system transforms the central domain of B to a central domain of A, surrounded by a ring of B. At $D \approx 5.6L_0$ there is another jump as the system creates a third layer of species A, surrounding a central domain of B. For larger pores, containing three lamellae of species A, it interesting that the inner two lamellae are only slightly compressed compared to the bulk period, while the outer two lamellae are highly compressed. This is consistent with our earlier suggestion that, for larger pores, the structure in the inner region of the pore should be similar to that in the bulk.

Experiments by Xiang et al. examined both symmetric and asymmetric PS-*b*-PBD diblock copolymer melts confined to cylindrical nanopores in an alumina membrane.[10] The PBD block preferentially segregated to the pore wall and can therefore be identified as the B block. Using an asymmetric copolymer, with a PS volume fraction of 0.64, they observed a structure similar to $\bar{C}_{1-6}$ in a pore of approximate diameter 140 nm (Figure 4 of ref 10). Using a symmetric copolymer, with a PS volume fraction of 0.44, they observed two concentric lamellar rings, similar to our L_2 structure, in an ~170 nm diameter pore (Figure 6 of ref 10). We estimate that $R_g \approx 7-8$ nm in these experiments; therefore, the $17R_g$ pore diameter used here is comparable the experimental pore diameter. The experiments of Sun et al., involving symmetric PS-*b*-PMMA ($R_g \approx 10$ nm), also observe the L_2 phase in 180 nm diameter pores.[11] Structures with nonhexagonal symmetry, such as the ones we predict here, have not been observed experimentally, to our knowledge. Our work suggests that such structures may exist for smaller values of f or higher temperatures than used in experiments. It is also possible that the nonuniform majority domain thickness required to form these nonhexagonally coordinated structures will cause them to become unstable in the axial direction and lead instead to the formation of three-dimensional morphologies (for example, cylindrical helices). The experiments of ref 10 observe that there are jumps in the number of concentric lamellae in the pore at specific pore diameters and that the confined lamellar period can be greater than the bulk period. These observations are consistent with Figure 6. Recently, structures with fewer lamellae or cylinders have been seen in smaller pores, consistent with our observation that simple space-packing constraints play a role in determining structure in these confined systems.[11,14]

In addition to the two-dimensional structures observed above, recent experiments suggest that three-dimensional structures can form in narrow pores (of diameter $\approx 4-6R_g$).[14,15] Furthermore, experiments with silica—surfactant systems, and corresponding SCMFT calculations for an AB diblock copolymer/C homopolymer blend confined to pores of various radii, observed helical, stacked toroid, and spherical structures.[16] It has been suggested that the stress due to confinement experienced by two-dimensional structures can lead to instability along the third dimension.[16] However, to date only a limited region of the phase diagram has been probed for three-dimensional structures, and the physical picture of these structures (for example, the range of stability, location of phase transition lines, and mechanism of formation) is far from complete. A SCMFT search for confined, three-dimensional structures which is as comprehensive as our two-dimensional study represents an extremely challenging problem and will require a significant increase in computational effort over the present study. Our two-dimensional study, in addition to describing experimentally observed

CDV

structures, will serve as a useful guide in the search for three-dimensional structures under confinement. Knowledge of possible two-dimensional structures is essential if one wishes to examine the important question of a possible stress-relief mechanism leading, for example, to the formation of helices from straight cylinders. We expect our two-dimensional results to apply to wide pores, but we expect that stress will lead to the formation of three-dimensional structures for smaller pore sizes. Also, we expect spherical domains to form when the composition of the copolymer is highly asymmetric. We are currently investigating how our phase diagram is modified when three-dimensional structures are allowed in the theory. Fluctuations, which are not included in the present mean-field treatment, may also modify the phase diagram.[28]

IV. Conclusions

To summarize, we have extensively explored the phase diagram of a diblock copolymer melt confined to a cylindrical nanopore through the use of real-space SCMFT. The phase diagram is more complicated than for the unconfined system, and we have found new two-dimensional structures not seen in the bulk, notably nonhexagonally coordinated cylindrical phases and structures intermediate between lamellae and cylinders. A major achievement of our work is that our map of the phase stability regions and phase transition curves now enables thermodynamic issues for this system, such as the nature of transitions between different structures, to be explored. Many trends in the phase diagram can be understood in terms of the ability of the system to pack domains into the finite-radius pore. For example, we observe that with decreasing pore diameter fewer cylinders can be accommodated. Our results are consistent with recent experimental observations, but we also predict a wealth of phases in parameter regions yet to be explored experimentally.

References and Notes

(1) Park, C.; Yoon, J.; Thomas, E. L. *Polymer* **2003**, *44*, 6725−6760.
(2) Park, M.; Harrison, C.; Chaikin, P. M.; Register, R. A.; Adamson, D. H. *Science* **1997**, *276*, 1401−1404.
(3) Segalman, R. A.; Yokoyama, H.; Kramer, E. J. *Adv. Mater.* **2001**, *13*, 1152−1155.
(4) Cheng, J. Y.; Mayes, A. M.; Ross, C. A. *Nat. Mater.* **2004**, *3*, 823−828.
(5) Matsen, M. W. *J. Chem. Phys.* **1997**, *106*, 7781−7791.
(6) Morkved, T. L.; Jaeger, H. M. *Europhys. Lett.* **1997**, *40*, 643−648.
(7) Geisinger, T.; Müller, M.; Binder, K. *J. Chem. Phys.* **1999**, *111*, 5241−5250.
(8) Huinink, H. P.; Brokken-Zijp, J. C. M.; van Dijk, M. A.; Sevink, G. J. A. *J. Chem. Phys.* **2002**, *112*, 2452−2462.
(9) Rasmussen, K. Ø. *J. Polym. Sci., Part B: Polym. Phys.* **2004**, *42*, 3695−3700.
(10) Xiang, H.; Shin, K.; Kim, T.; Moon, S. I.; McCarthy, T. J.; Russell, T. P. *Macromolecules* **2004**, *37*, 5660−5664.
(11) Sun, Y.; Steinhart, M.; Zschech, D.; Adhikari, R.; Michler, G. H.; Gösele, U. *Macromol. Rapid Commun.* **2005**, *26*, 369−375.
(12) He, X.; Song, M.; Liang, H.; Pan, C. *J. Chem. Phys.* **2001**, *114*, 10510−10513.
(13) Sevink, G. J. A.; Zvelindovsky, A. V.; Fraaije, J. G. E. M.; Huinink, H. P. *J. Chem. Phys.* **2001**, *115*, 8226−8230.
(14) Shin, K.; Xiang, H.; Moon, S. I.; Kim, T.; McCarthy, T. J.; Russell, T. P. *Science* **2004**, *306*, 76.
(15) Xiang, H.; Shin, K.; Kim, T.; Moon, S. I.; McCarthy, T. J.; Russell, T. P. *Macromolecules* **2005**, *38*, 1055−1056.
(16) Wu, Y.; Cheng, G.; Katsov, K.; Sides, S. W.; Wang, J.; Tang, J.; Fredrickson, G. H.; Moskovits, M.; Stucky, G. D. *Nat. Mater.* **2004**, *3*, 816−822.
(17) Matsen, M. W.; Schick, M. *Phys. Rev. Lett.* **1994**, *72*, 2660−2663.
(18) Matsen, M. W. *J. Phys.: Condens. Matter* **2002**, *14*, R21−R47.
(19) Helfand, E. *J. Chem. Phys.* **1975**, *62*, 999−1005.
(20) Hong, K. M.; Noolandi, J. *Macromolecules* **1981**, *14*, 727−736.
(21) Drolet, F.; Fredrickson, G. H. *Phys. Rev. Lett.* **1999**, *83*, 4317−4320.
(22) Tzeremes, G.; Rasmussen, K. Ø.; Lookman, T.; Saxena, A. *Phys. Rev. E* **2002**, *65*, 041806-1−041806-5.
(23) While the *absolute* free energies of the structures are sensitive to the discretization used, the *differences* between free energies are only slightly influenced by discretization. As a consequence, the phase boundaries are not significantly changed. In our study of intermediate structures, we find that the shift in the absolute free energies is smaller on going from a 256 × 256 lattice to a 512 × 512 lattice than it is on going from a 128 × 128 lattice to a 256 × 256 lattice.
(24) Operationally, this means that for lattice points closer to the origin than the pore radius R, incompressibility, eq 8, is enforced. For lattice points at or farther than R from the origin, eq 8 is not satisfied and $\phi_A = \phi_B = q = q^\dagger = 0$ is *imposed* at these lattice points. We have chosen this approach over other approaches which use incompressibility conditions that smoothly approach zero as the pore wall is approached (ref 5, for example) for simplicity.
(25) Press, W. H.; Teukolsky, S. A.; Vetterling, W. T.; Flannery, B. P. *Numerical Recipes in C: The Art of Scientific Programming*, 2nd ed.; Cambridge University Press: New York, 1997.
(26) We caution the reader that we use the word "cylinders" only as a convenient term to describe these domains. Although these structures exist in a parameter region that overlaps with the region where hexagonally coordinated cylinders are in equilibrium in the bulk phase diagram, our two-dimensional study does not determine whether in three dimensions, under confinement, these domains are cylinders, spheres, helices, or some other three-dimensional morphology.
(27) Wickham, R. A.; Garbary, R. A., unpublished results. Miao, B.; Yan, D.; Shi, A.-C.; Wickham, R. A., unpublished results.
(28) Fredrickson, G. H.; Helfand, E. *J. Chem. Phys.* **1987**, *87*, 697−705.